Aeroacoustics Conferences
June 4-7, 2024, Rome, Italy
30th AIAA/CEAS Aeroacoustics Conference (2024)

10.2514/6.2024-3376

Modelling Offset Dual-Stream Jet Noise Using an Acoustic Analogy and Input from Steady RANS

Shabeeb N. P.* and Aniruddha Sinha†
Department of Aerospace Engineering, Indian Institute of Technology Bombay, Powai, Mumbai, 400076, INDIA

This paper presents a methodology for predicting offset dual-stream jet noise using steady RANS solutions. The acoustic analogy relies on the linearized Euler equations, incorporating Lilley's acoustic analogy with a locally parallel mean flow assumption. Lilley's equation for a non-axisymmetric jet is solved in the physical domain for each axial location separately. Axisymmetric jet Green's function results are used to validate our approach, and they are found to match exactly. Smooth transitions of the Green's function with eccentricity and observer azimuthal location are observed. Steady RANS simulations are conducted for single-stream, dual-stream axisymmetric, and offset jets. The far-field noise predicted from the RANS data matches the corresponding experimental results present in the literature.

I. Introduction

Jet noise is one of the most challenging fluid mechanics problems that researchers have been working on for the last few decades and it is also one of the loudest noises ever produced by mankind. The introduction of turbofan engines with progressively higher bypass ratios has successfully decreased jet noise by a significant margin. However, achieving further reductions in jet noise while maintaining other performance characteristics presents an immense challenge. Extensive research has focused on the development of quieter nozzle designs. This task is challenging due to cost constraints and the complex nature of the flow field. Gaining a comprehensive understanding of the flow field and identifying the sources of jet noise will serve as a guide for creating noise prediction tools and may ultimately lead to the realization of quieter designs.

Although axisymmetric (round) jets constitute a benchmark flow for their azimuthal homogeneity, practical prerogatives dictate the prevalence of non-axisymmetric jets in engines. The azimuthal inhomogeneity of such jets may be preferred, either for promoting mixing to reduce noise radiation, or for redirecting the noise away from the bottom sector of the jet. The former is exemplified by jets exiting from nozzles with chevrons [1], and by jets from round nozzles having additional micro-jets impinging at their lip [2]. An instance of the latter is a dual-stream jet where the two round streams are not coaxial, but instead have an offset between them such that the secondary potential core is thickened in the bottom sector (see fig. 1). In the present work, we are motivated by several research efforts that have experimentally investigated such offset dual-stream jets [3–8]; appreciable preferential noise reduction has been reported in the sector shielded by the thicker secondary potential core.

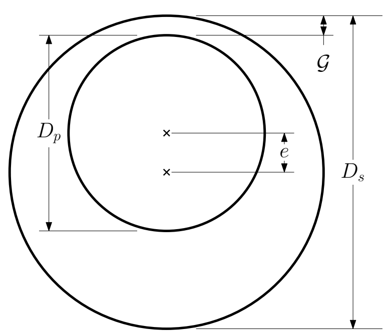

Fig. 1 **Schematic of nozzle arrangement for offset dual-stream round jets.**

We pursue the modelling of noise radiated from such non-axisymmetric jets, extending earlier models formulated for axisymmetric jets [9–14]. The earlier models developed are based on the solution of Lilley's equation for an

*Doctoral student; AIAA Student Member
†Associate Professor; AIAA Member; Corresponding author: as@aero.iitb.ac.in

axisymmetric jet with a locally parallel mean flow assumption to account for the propagation of sound through a jet plume. Then, the far-field noise is predicted by convolving Lilley's Green's function with the noise sources, where the input data comes from a steady RANS solution. The same methodology has been used to predict noise radiated from chevron jets, using the axisymmetric Lilley's Green's function and a non-axisymmetric RANS solution from the corresponding chevron jet in Ref. [13]. Papamoschou [15] developed a methodology for predicting far-field noise radiated from offset jets based on Lighthill's acoustic analogy and input data from a RANS solution. In this work, we use Lilley's acoustic analogy for a non-axisymmetric jet with a locally parallel mean flow assumption and take the mean flow field from a steady Reynolds-averaged Navier Stokes (RANS) simulation. The mathematical formulation for the noise prediction scheme we are proposing for non-axisymmetric jets is detailed in the subsequent section. The approach is sought to be validated against the existing experimental data for the offset dual-stream round jets cited above. The ultimate goal is to obtain a tool for rapid aeroacoustic design of such jets.

II. Predicting noise from a non-axisymmetric jet

Our mathematical formulation of the jet noise prediction model is based on the works of Refs. [9–14]. We extend these axisymmetric jet formulations to the non-axisymmetric offset dual-stream round jets under investigation here.

A. The forced acoustic wave equation

The governing equations are the Euler equations as viscous effects are deemed unimportant for both sound generation and propagation. The equations are

$$\frac{D\pi}{Dt} + \boldsymbol{\nabla}\cdot\boldsymbol{u} = 0, \qquad \frac{D\boldsymbol{u}}{Dt} + a^2\boldsymbol{\nabla}\pi = 0. \tag{1}$$

where $\boldsymbol{u}$ is the velocity vector, a is the local speed of sound and $\pi := \gamma^{-1}\ln(p/p_\infty)$ is the logarithmic pressure, and $D(\cdot)/Dt := \partial/\partial t + \boldsymbol{u}\cdot\boldsymbol{\nabla}$ is the material derivative. The Euler equations are linearized by expanding the flow variables as fluctuations (indicated by a prime) on a time-averaged base state (indicated by an overline). Introducing the base flow material derivative $\overline{D}/\overline{D}t := \partial/\partial t + \overline{\boldsymbol{u}}\cdot\boldsymbol{\nabla}$, these equations are re-written as

$$\frac{\overline{D}\pi'}{\overline{D}t} + \boldsymbol{\nabla}\cdot\boldsymbol{u}' = -\boldsymbol{u}'\cdot\boldsymbol{\nabla}\pi' =: f_0, \qquad \frac{\overline{D}\boldsymbol{u}'}{\overline{D}t} + \boldsymbol{u}'\cdot\boldsymbol{\nabla}\overline{\boldsymbol{u}} + \overline{a^2}\boldsymbol{\nabla}\pi' = -\boldsymbol{u}'\cdot\boldsymbol{\nabla}\boldsymbol{u}' - \left(a^2\right)'\boldsymbol{\nabla}\pi' =: \boldsymbol{f}. \tag{2}$$

The nonlinear terms in the RHS constitute noise sources for the linearized propagation problem in the LHS. The linearized Euler equations (LEE) may be solved by convolving its vector Green's function with the source.

In jet acoustics, it is common to assume that the base flow is locally parallel due to the slow spread rate of typical jets. Considering such a locally parallel mean flow for a non-axisymmetric jet, then simplifies the LEE to the so-called Lilley's equation [16]. The equations are expressed in cylindrical coordinates (x, r, ϕ) since axisymmetric jets form the baseline for this study. The Lilley's operator acting on the logarithmic pressure component of the vector Green's function of the LEE ($\widehat{\pi}_g^n$) in the temporal Fourier domain can then be written as

$$\begin{aligned}
&\left(\overline{D}_\omega^3 - \overline{a^2}\,\overline{D}_\omega\nabla^2 - \frac{\partial\overline{a^2}}{\partial r}\overline{D}_\omega\frac{\partial}{\partial r} - \frac{1}{r^2}\frac{\partial\overline{a^2}}{\partial\phi}\overline{D}_\omega\frac{\partial}{\partial\phi} + 2\overline{a^2}\frac{\partial\overline{u}}{\partial r}\frac{\partial^2}{\partial x\partial r} + \frac{2\overline{a^2}}{r^2}\frac{\partial\overline{u}}{\partial\phi}\frac{\partial^2}{\partial x\partial\phi}\right)\widehat{\pi}_g^n(\boldsymbol{x}|\boldsymbol{x}_s;\omega) \\
&\quad = \overline{D}_\omega^2\delta(\boldsymbol{x}-\boldsymbol{x}_s)\,\delta_{0n} - \overline{D}_\omega\frac{\partial}{\partial x}\delta(\boldsymbol{x}-\boldsymbol{x}_s)\,\delta_{xn} - \left[\frac{1}{r}\overline{D}_\omega\frac{\partial}{\partial r}\left(r\delta(\boldsymbol{x}-\boldsymbol{x}_s)\right) - 2\frac{\partial\overline{u}}{\partial r}\frac{\partial}{\partial x}\delta(\boldsymbol{x}-\boldsymbol{x}_s)\right]\delta_{rn} \\
&\qquad - \left[\frac{1}{r}\overline{D}_\omega\frac{\partial}{\partial\phi} - \frac{2}{r}\frac{\partial\overline{u}}{\partial\phi}\frac{\partial}{\partial x}\right]\delta(\boldsymbol{x}-\boldsymbol{x}_s)\,\delta_{\phi n} =: \mathscr{S}^n(\boldsymbol{x}-\boldsymbol{x}_s;\omega),
\end{aligned} \tag{3}$$

where the operator on the LHS is Lilley's wave operator, $\overline{u}$ is the mean velocity component in the streamwise (i.e., x) direction, and $\overline{D}_\omega := -i\omega + \overline{u}\partial/\partial x$. The vector Green's functions are indexed by n, which takes values in $\mathscr{N} := \{0, x, r, \phi\}$ corresponding to forcing of the conservation equations for mass and three cylindrical components of momentum, respectively (see eqn. (2)). As indicated, the RHS constitutes the source in this acoustic analogy.

Let us denote the (scalar) Green's function of Lilley's wave operator by $\widehat{g}(\boldsymbol{x}|\boldsymbol{x}_s;\omega)$. The notation implies that it is the response at $\boldsymbol{x}$ due to a unit point harmonic source at $\boldsymbol{x}_s$ at circular frequency ω. Then, the solution to eqn. (3) can be formally written as

$$\widehat{\pi}_g^n\left(\boldsymbol{x}|\boldsymbol{x}_s;\omega\right)=\iiint\widehat{g}\left(\boldsymbol{x}|\boldsymbol{x}_t;\omega\right)\mathscr{S}^n(\boldsymbol{x}_t-\boldsymbol{x}_s;\omega)d\boldsymbol{x}_t. \tag{4}$$

B. Solving Lilley's equation for a non-axisymmetric jet

The numerical solution to the Green's function of Lilley's equation for axisymmetric jets has been pursued using the adjoint approach [12, 17], and we do the same for the non-axisymmetric jets under investigation here. In the adjoint problem, we consider a point harmonic source at the far away observer locations, and seek the corresponding acoustic results in the jet flow region. Denoting the adjoint Green's function of Lilley's equation as $\widehat{g}_a\left(\boldsymbol{x}_s|\boldsymbol{x};\omega\right)$, one can find its governing equation as

$$\Bigg[\overline{D}_{a,\omega}^3-\overline{a^2}\,\overline{D}_{a,\omega}\nabla^2-\frac{\partial\overline{a^2}}{\partial r}\overline{D}_{a,\omega}\frac{\partial}{\partial r}-\frac{1}{r^2}\frac{\partial\overline{a^2}}{\partial\phi}\overline{D}_{a,\omega}\frac{\partial}{\partial\phi}+4\overline{a^2}\frac{\partial\overline{u}}{\partial r}\frac{\partial^2}{\partial x\partial r}+\frac{4\overline{a^2}}{r^2}\frac{\partial\overline{u}}{\partial\phi}\frac{\partial^2}{\partial x\partial\phi}+\frac{3}{r}\frac{\partial}{\partial r}\left(r\overline{a^2}\frac{\partial\overline{u}}{\partial r}\right)\frac{\partial}{\partial x}$$
$$+\frac{3}{r^2}\frac{\partial}{\partial\phi}\left(\overline{a^2}\frac{\partial\overline{u}}{\partial\phi}\right)\frac{\partial}{\partial x}\Bigg]\widehat{g}_a\left(\boldsymbol{x}|\boldsymbol{x}_0;\omega\right)=\delta\left(\boldsymbol{x}-\boldsymbol{x}_0\right), \tag{5}$$

where $\overline{D}_{a,\omega}=-i\omega+\overline{u}\partial/\partial x$.

The adjoint sound propagation problem is broken down into two parts: outside the jet where there is no flow, and inside the jet where there is sheared flow. The demarcation is conveniently chosen as the radial location $r=r_0$ where the mean flow field gradient is below a certain threshold (e.g., a sufficiently small fraction of the center-line value). The 'outer' solution of the adjoint problem for axisymmetric jets is the sum of the direct part of the solution (essentially a plane wave) and the scattered part of the solution [12, 17]; these remain essentially identical in form in our non-axisymmetric jet also. That is, the outer solution can be written as

$$\underset{r\geq r_0}{\widehat{g}_a}\left(\boldsymbol{x}|\boldsymbol{x}_0;\omega\right)=\frac{i\mathrm{e}^{i\omega(R_0-x\cos\Theta_0)/a_\infty}}{4\pi\omega a_\infty^2R_0}\sum_{m=-\infty}^{\infty}(-i)^m\left[J_m\left(\frac{\omega\sin\Theta_0}{a_\infty}r\right)+A_mH_m^{(1)}\left(\frac{\omega\sin\Theta_0}{a_\infty}r\right)\right]\mathrm{e}^{im(\phi-\phi_0)}. \tag{6}$$

Here, $\boldsymbol{x}_0=(R_0,\Theta_0,\phi_0)$ is the observer location in spherical coordinates, whose origin is centered on the primary jet nozzle at its exit plane, with the polar axis being along the downstream jet axis. Further, J_m is the m^{th}-order Bessel function of the first kind, accounting for the direct part. Moreover, $H_m^{(1)}$ is the m^{th}-order Hankel function of the first kind that accounts for the scattered part, with A_m as arbitrary constants at this stage that will be determined subsequently by matching with the inner solution. Note that for axisymmetric jets, the azimuthal coordinate ϕ_0 of the far-field (adjoint) point source was taken to be zero without loss of generality. This simplification cannot be made in our case due to the lack of axisymmetry in the mean flow field. Moreover, symmetry considerations led to the relation $A_{-m}=A_m$ in axisymmetric jets, which does not extend to general non-axisymmetric jets.

Guided by the form of the outer solution in eqn. (6), and following the earlier works on axisymmetric jets [12, 17], we consider the following ansatz for the inner solution:

$$\underset{r\leq r_0}{\widehat{g}_a}\left(\boldsymbol{x}|\boldsymbol{x}_0;\omega\right)=\frac{i\mathrm{e}^{i\omega(R_0-x\cos\Theta_0)/a_\infty}}{4\pi\omega a_\infty^2R_0}\widehat{f}(r,\phi,\phi_0;\omega,x). \tag{7}$$

Substituting eqn. (7) in eqn. (5), we have the governing equation for $\widehat{f}(r,\phi,\phi_0;\omega,x)$ as

$$\frac{1}{r}\frac{\partial}{\partial r}\left(r\frac{\partial\widehat{f}}{\partial r}\right)+\frac{1}{r^2}\frac{\partial^2\widehat{f}}{\partial\phi^2}-\left(\frac{4\cos\Theta_0}{a_\infty-\overline{u}\cos\Theta_0}\frac{\partial\overline{u}}{\partial r}+\frac{1}{\overline{\rho}}\frac{\partial\overline{\rho}}{\partial r}\right)\frac{\partial\widehat{f}}{\partial r}-\frac{1}{r^2}\left(\frac{4\cos\Theta_0}{a_\infty-\overline{u}\cos\Theta_0}\frac{\partial\overline{u}}{\partial\phi}+\frac{1}{\overline{\rho}}\frac{\partial\overline{\rho}}{\partial\phi}\right)\frac{\partial\widehat{f}}{\partial\phi}+\Bigg[-\frac{\omega^2\cos^2\Theta_0}{a_\infty^2}$$
$$+\omega^2\frac{(1-\cos\Theta_0\overline{u}/a_\infty)^2}{\gamma p_\infty/\overline{\rho}}-\frac{3\cos\Theta_0}{a_\infty-\overline{u}\cos\Theta_0}\left\{\frac{1}{r}\frac{\partial}{\partial r}\left(r\frac{\partial\overline{u}}{\partial r}\right)+\frac{1}{r^2}\frac{\partial^2\overline{u}}{\partial\phi^2}-\frac{1}{\overline{\rho}}\left(\frac{\partial\overline{\rho}}{\partial r}\frac{\partial\overline{u}}{\partial r}+\frac{1}{r^2}\frac{\partial\overline{\rho}}{\partial\phi}\frac{\partial\overline{u}}{\partial\phi}\right)\right\}\Bigg]\widehat{f}=0. \tag{8}$$

This is a two-dimensional PDE that has to be solved numerically. It is noted that the governing equation has a critical point at $r=0$, and a critical layer for all (r,ϕ) such that $\overline{u}(r,\phi)\cos\Theta_0=a_\infty$. Methods for addressing the critical point and critical layer will be discussed at the end of this section.

Our choice of formulating the governing equation for $\widehat{f}$ in polar coordinates results in an artificial boundary (or a critical point) at $r = 0$, where an appropriate boundary condition has to be deviced now. Recall that the flows of interest are coaxial and eccentric dual-stream round jets. The point of maximum mean streamwise velocity might not be at $r = 0$ for eccentric jets. Here, we assume that the mean flow velocity and density reach their extremes, and their radial and azimuthal derivatives approach zero as $r \rightarrow 0$. Then, it can be shown [17, 18] that the m^{th} Fourier azimuthal mode of the inner solution behaves as $r^{|m|}$ near the origin. For practical purposes, we limit the azimuthal Fourier decomposition to $m \in [-M, M]$. Then, we have the 'center-line' boundary condition as

$$\widehat{f}(r, \phi - \phi_0; \omega) = \sum_{m=-M}^{M} a_m r^{|m|} \mathrm{e}^{im(\phi-\phi_0)}, \qquad \frac{\partial \widehat{f}}{\partial r}(r, \phi - \phi_0; \omega) = \sum_{m=-M}^{M} |m| a_m r^{|m|-1} \mathrm{e}^{im(\phi-\phi_0)}, \qquad r \rightarrow 0. \quad (9)$$

Here, $\{a_m\}_{m=-M}^{M}$ are $(2M + 1)$ constants that are arbitrary at this stage. As in the case of the outer solution, for axisymmetric jets we have the symmetry $a_{-m} = a_m$ that does not carry over to the present non-axisymmetric jets.

The solution procedure starts by fixing the constants a_m (more about this later). A central difference scheme is applied in the azimuthal direction using a uniform ϕ-grid, say. This converts eqn. (8) from a two-dimensional PDE to a set of coupled second-order ODEs in r – as many as there are ϕ grid points. The conversion from a second-order ODE in r to a coupled set of two first-order ODEs in r is standard. The resulting set of coupled first-order ODEs may be integrated in the radial direction starting from the above center-line boundary condition. We use the `ode45` function of MATLAB to leverage its variable step-size approach.

Let $\widehat{f_m}(r, \phi, \phi_0; \omega, x)$ denote the inner solution obtained by setting $a_m = 1$ and all other $2M$ a's to zero in eqn. (9). Essentially, $\widehat{f_m}$ has the azimuthal behaviour corresponding to the m^{th} Fourier azimuthal mode near the origin. Of course, the non-axisymmetry of the mean flow field results in a rich azimuthal Fourier spectrum in the solution over the remainder of the radial domain. Evidently, we can calculate $(2M + 1)$ such linearly independent inner solutions. Then, an arbitrary inner solution can be composed as a linear combination of these: $\widehat{f} = \sum_{m=-M}^{M} a_m \widehat{f_m}$.

The radial integration of the inner solution stops at the interfacial point $r = r_0$. Here, the solution on the circumferential grid needs to be matched with the outer solution of eqn. (6). To have a well-posed problem, we solve the inner solution on a uniform circumferential grid having $(2M + 1)$ grid points. Further, we express the outer solution with the same Fourier azimuthal modal richness as the inner solution; i.e., the unknowns in eqn. (6) are $\{A_m\}_{m=-M}^{M}$. Then, the matching of the adjoint Lilley's Green's function's inner and outer parts, as well as their radial derivatives, at the interface $r = r_0$ yields a set of $(4M + 2)$ linear equations in as many unknowns, which may be solved uniquely.

As we discussed above, we have the critical layer at $r = 0$ and $a_\infty - \overline{u}\cos\Theta_0 = 0$. We start our integration at $r \rightarrow 0$ to avoid the critical layer. To avoid the singularity at $a_\infty - \overline{u}\cos\Theta_0 = 0$, we have to deform the r-integration contour around the singularity into the complex domain using, say, a Gaussian profile [19]. In general, the radial location of the singularity will vary with the azimuthal location. To solve the governing eqn. (8), consistent radial grid points across all azimuthal directions are required. Due to these challenges, we have not predicted the far-field noise for observer locations that falls within the singularity. In our future work, we aim to extend this research to address the singularity at the critical layer. Our plan involves employing the contour deformation method mentioned earlier, ensuring that all critical points lie comfortably within the deformed radial grid. This approach will yield a uniform radial grid across all azimuthal directions, with the contour deformed around the critical layer.

Once we have the adjoint Green's function, which is the same as the direct Green's function for this problem [17], the pressure components of the four vector Green's functions of LEE are determined using eqn. (4).

C. Modelling of sources

The modelling procedure for the sound sources follow identically from the axisymmetric jet case [9, 11, 14, 20]. The only difference is that the sound source field will be non-axisymmetric, so that the source parameters will have to be retrieved from the RANS solution separately for each azimuthal angle, instead of being averaged over the circumference. We briefly outline the procedure below, highlighting the main differences.

Since we are invariably interested only in the spectral density of the pressure (and not its time history), only the spatio-temporal cross-correlations of the source terms in eqn. (2) have to be modelled [13]. Based on extensive round jet databases accumulated over decades, such a model has been proposed by many researchers [9, 11, 20], and is of the form

$$\langle f_n(\boldsymbol{x}, t) f_{n'}(\boldsymbol{x} + \boldsymbol{\eta}, t + \tau) \rangle_t = \delta_{nn'} A_n(\boldsymbol{x}) \exp\left\{ -\frac{|\tau|}{\tau_s(\boldsymbol{x})} - \frac{(\eta_x - \overline{u}(\boldsymbol{x})\tau)^2}{\ell_x^2(\boldsymbol{x})} - \frac{\eta_y^2}{\ell_y^2(\boldsymbol{x})} - \frac{\eta_z^2}{\ell_z^2(\boldsymbol{x})} \right\}, \quad n, n' \in \mathcal{N}. \qquad (10)$$

Here, for convenience of modelling, we have switched to Cartesian coordinates for the spatial separation vector $\boldsymbol{\eta} := \eta_x \hat{\boldsymbol{i}} + \eta_y \hat{\boldsymbol{j}} + \eta_z \hat{\boldsymbol{k}}$. At zero-time lag, this ansatz posits a Gaussian decay of the two-point cross-correlation in all three Cartesian coordinate directions, albeit with different length scales ℓ_x, ℓ_y, ℓ_z. Moreover, it invokes the frozen field hypothesis and models an exponential decay of correlation with time, having time scale τ_s, if one were to move with the mean flow (assumed negligible in the cross-stream directions for this purpose). Further, it is assumed that each source term is correlated only with itself and is uncorrelated with all other source terms. Finally, the model assumes the behavior of the correlation terms to be the same for all the sources, albeit with different amplitudes that are related by dimensional analysis to the local velocity scale u_s and the above length and time scales as

$$A_0(\boldsymbol{x}) = B_0^2 \frac{(u_s(\boldsymbol{x})/a_\infty)^4}{\tau_s^2(\boldsymbol{x})}, \qquad A_n(\boldsymbol{x}) = B_{>0}^2 \frac{(u_s(\boldsymbol{x})/a_\infty)^2 u_s^4(\boldsymbol{x})}{\ell_x^2(\boldsymbol{x})}, \quad n \in \{x, r, \phi\}. \tag{11}$$

Here, B_0 and $B_{>0}$ are empirical constants.

In a steady RANS-based noise prediction model, the local length, time and velocity scales are determined from the local mean turbulent kinetic energy $\overline{K}(\boldsymbol{x})$ and dissipation $\overline{\epsilon}(\boldsymbol{x})$ using simple scaling laws [9–13]:

$$u_s(\boldsymbol{x}) = c_u \sqrt{\frac{2}{3}\overline{K}(\boldsymbol{x})}, \qquad \tau_s(\boldsymbol{x}) = c_\tau \frac{\overline{K}(\boldsymbol{x})}{\overline{\epsilon}(\boldsymbol{x})}, \qquad \ell_x(\boldsymbol{x}) = c_\ell \frac{\{\overline{K}(\boldsymbol{x})\}^{3/2}}{\overline{\epsilon}(\boldsymbol{x})}, \qquad \ell_y(\boldsymbol{x}) = \ell_z(\boldsymbol{x}) = \frac{\ell_x(\boldsymbol{x})}{3}. \tag{12}$$

where, c_ℓ, c_τ and c_u are empirical constants. The values of these constants arfe chosen to be 0.4, 0.06 and 1.0 respectively following the work of Miller [13].

Subsequently, we would need to model the source cross-correlations presented in eqn. (10) in the frequency domain. Although all the other scales carry over from their time-averaged counterparts modelled above, the turbulent length scales can be expected to depend on the frequency. Corresponding to the radial frequency ω, the Strouhal number is defined as $St = \omega D_j/(2\pi U_j)$, where D_j is the jet's nozzle-exit diameter, and U_j is its nozzle-exit velocity. In Ref. [21], the frequency-dependent length scales were modelled as (note the subtle change in notation from the frequency-independent variants)

$$l_i(\boldsymbol{x}, \omega) = \ell_i(\boldsymbol{x}) \frac{1 - \mathrm{e}^{-c_f St}}{c_f St}, \quad \forall i \in \{x, y, z\}. \tag{13}$$

The empirical constant $c_f = 11.25$ was chosen to match the experimental observations [21]. In our recent work [14], we have proposed an improved alternative to the above model given as,

$$l_i(\boldsymbol{x}, St) = \ell_i(\boldsymbol{x}) \frac{2D_j}{St\, x} \frac{1 - \exp\{-c_f St\}}{1 - \exp\{-2c_f D_j/x\}}. \tag{14}$$

where D_j is the jet exit diameter for single stream jet and primary jet exit diameter for the dual-stream jet.

The above expressions do not explicitly discriminate between axisymmetric and non-axisymmetric jets. The only implicit difference is that the mean TKE and dissipation fields being general three-dimensional fields in non-axisymmetric jets, the length, time and velocity scales derived therefrom also have variations in all three coordinate directions. Thus, the two-point correlation of the noise sources in eqn. (10) are functions of all three directions in the reference coordinate $\boldsymbol{x}$. On the other hand, in axisymmetric jets, all these quantities cease to be functions of the azimuthal coordinate.

D. The far-field spectrum

Assuming that the observer is in the far field, and that the vector Green's function of two closely-placed source points differ only by a phase factor [9], the relevant spectral density of pressure fluctuations can be approximated as

$$\begin{aligned} S_p(\boldsymbol{x}_0, \omega) &= 2\pi^{3/2} (\gamma p_\infty)^2 \sum_{n \in \mathcal{N}} \iiint \left| \widehat{\pi}_g^n (\boldsymbol{x}_0 | \boldsymbol{x}_s; \omega) \right|^2 \sigma_n(\boldsymbol{x}_s; \boldsymbol{x}_0, \omega) d\boldsymbol{x}_s, \\ \sigma_n(\boldsymbol{x}_0; \boldsymbol{x}, \omega) &:= A_n(\boldsymbol{x}_s) \frac{l_x^3(\boldsymbol{x}_s; \omega)}{9} \tau_s(\boldsymbol{x}_s) \frac{\exp\{-\omega^2 (1 + 8\cos^2\Theta_0) l_x^2(\boldsymbol{x}_s; \omega)/(36 a_\infty^2)\}}{1 + \omega^2 \tau_s^2(\boldsymbol{x}_s)(1 - \overline{u}(\boldsymbol{x}_s)\cos\Theta_0/a_\infty)^2}. \end{aligned} \tag{15}$$

In the above, the frequency-dependent length scales are introduced, and the relation between the cross-stream and streamwise length scales presented in eqn. (12) is used implicitly.

RANS Case	M_p	U_p	ρ_p/ρ_∞	M_s	U_s	D_s/D_p	Configuration	Grid size	Reference
C17M90-1	1.5	430	1.45	0.9	290	1.7	Coaxial	5.16×10^4	Murakami
C17M90-2	1.5	430	1.45	0.9	290	1.7	Coaxial	1.3×10^5	and
E17M90	1.5	430	1.45	0.9	290	1.7	Eccentric	1.24×10^6	Papamoschou [4]
Single	1.5	700	0.59	-	-	-	Single-steam	6.43×10^4	Papamoschou
COAX1	1.5	700	0.59	1.0	360	1.4	Coaxial	5.32×10^4	and
ECC-1	1.5	700	0.59	1.0	360	1.4	Eccentric	1.29×10^6	Debiasi [3]
ECC-2	1.5	700	0.59	1.0	360	1.4	Eccentric	1.72×10^6	

Table 1 **Test cases of steady RANS simulation.**

Reference	Cases	Velocity profile	Centerline Mach number	SPL	OASPL
Murakami	C17M90	✓	-	-	-
and	E17M90	✓	-	-	-
Papamoschou [4]					
Papamoschou	Single	-	✓	$\Theta_0 = 40^0, 45^0, 90^0$	✓
and	COAX1	-	✓	$\Theta_0 = 45^0, 90^0$	-
Debiasi [3]	ECC	-	✓	$(\Theta_0 = 40^0, \phi_0 = 0^0)$	-
				$(\Theta_0 = 45^0, \phi_0 = 135^0)$	✓
				$(\Theta_0 = 45^0, \phi_0 = 150^0)$	✓
				$(\Theta_0 = 40^0, 45^0, 90^0, \phi_0 = 180^0)$	✓

Table 2 **Experimental data available for validation**

III. Results

We present both the mean flow and far-field results obtained from the steady RANS simulations of single-stream, dual-stream coaxial and dual-stream eccentric jets, as well as their validation against experimental data.

A. Steady RANS simulation

To predict far-field jet noise using the model described in the previous sections, we conducted steady Reynolds-averaged Navier-Stokes (RANS) simulations for single-stream jets, as well as dual-stream coaxial and eccentric jets. Since the noise source model is developed based on a $K - \epsilon$ model, employing a RANS simulation with the same model is the obvious choice. However, the literature indicates that the standard $K - \epsilon$ model is unable to predict the mean flow of turbulent axisymmetric jets very accurately [22]. This discrepancy arises because the standard coefficients were calibrated using boundary-layer and low Mach number planar mixing layer data, whose turbulence characteristics do not entirely align with those of high-speed jets. Ref. [23] introduced a new set of empirical coefficients and demonstrated that the model can accurately predict axisymmetric, rectangular, and elliptic jet mean flows across a wide range of Mach numbers and temperature ratios.

To validate both the mean flow data and the far-field noise prediction, we refer to experimental results reported in the literature [3, 4]. The jets we simulated and the corresponding experimental data available for validation are summarized in Table 2. We have maintained consistent nomenclature with the reference papers. From Table 2, it is evident that we lack cases where we can validate both mean flow and far-field sound. Hence, we utilize available velocity profiles and centerline Mach number distributions to validate our RANS simulation.

Details of the simulated test cases are summarized in Table 1, where $(\cdot)_p$ denotes primary jet parameters and $(\cdot)_s$ denotes secondary jet parameters. Steady RANS simulations were performed using the OpenFOAM toolbox. C17M90 and E17M90 cases are cold jets with a dual-stream configuration. The primary jet is Mach 1.5, and the secondary jet is Mach 0.9. Additionally, a heated single-stream jet with Mach 1.5, denoted as 'Single' in Table 1, was simulated. All other cases are heated jets with dual-stream configurations, where primary and secondary Mach numbers are 1.5 and

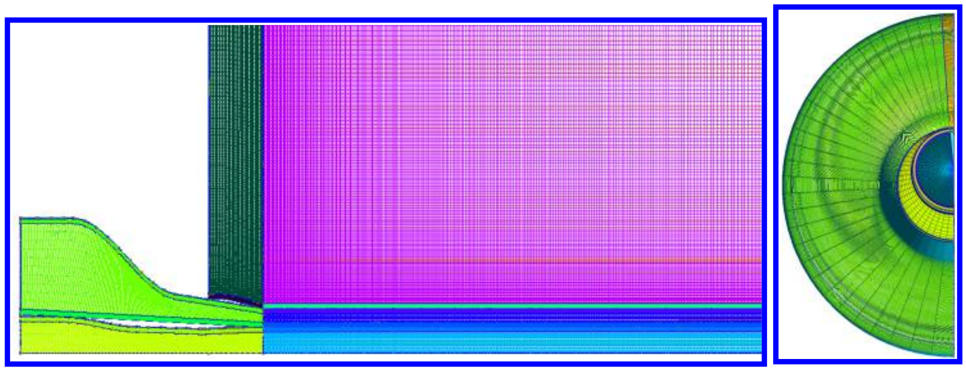

Fig. 2 **Mesh near the nozzle exit for (a) C17M90-2 and (b) ECC-2 cases.**

1.0, respectively. The primary jet exit diameter is $D_p = 12.7$ mm for all cases, and the secondary to primary diameter ratio is provided in Table 1. Note that in their terminology, an eccentric jet is maximally offset, i.e., the primary and secondary nozzles are touching at one point so that $e = (D_s - D_p)/2$ in fig. 1; the two nozzles share the same exit plane.

We have used the method of characteristic nozzle for the primary jet and the 'SMC000' nozzle [1] for the secondary jet (just because it is a well-designed subsonic jet nozzle). We have included the nozzle geometry in the flow domain. For the axisymmetric cases, a single-celled 5° azimuthal wedge has been generated in the $x - r$ flow domain. For the eccentric case, the azimuthal domain extends over 180°, since there is a mirror symmetry of the mean flow field about the plane containing the center-line of the primary jet and the point of minimum approach between the two nozzles. The radial domain extends to $12D_p$ for all the jets. The axial domain extends to $25D_p$ downstream of the nozzle exit all the jets, except ECC-1 and ECC-2. For the eccentric jets, the axial extent of the domain used were $20D_p$ and $30D_p$ for ECC-1 and ECC-2 cases respectively.

The changes made in the domain extent for the eccentric jets are discussed later. Replicating the completely eccentric configuration of the reference causes issues in meshing. So, with reference to fig. 1, we keep a minimum gap of $\mathcal{G} = 0.01D_p$ between the two nozzles at their exit plane. A three-dimensional structured mesh has been created using the Gmsh [24] meshing tool, consisting of hexahedral and prism elements. The simulation for the C17M90 jet was performed on two meshes so as to investigate its grid-independence (as indicated in Table 1); the finer one is depicted in fig. 2(a). The mesh is refined selectively where the gradients are higher – radially near the nozzles' walls, radially along the two lip-lines, and axially in the vicinity of the nozzle exit plane.

The operating conditions are controlled by the nozzle pressure ratio and nozzle temperature ratio at the inlet of the primary and secondary nozzles. The external inlet outside the secondary nozzle and the radial far-field boundary of the domain are treated as inlets with freestream conditions. The far downstream end of the flow domain is treated as the outlet with freestream pressure condition. On the nozzle walls, we have no-slip velocity and zero-gradient pressure and temperature boundary conditions. In the steady RANS solver we have used the second order accurate Green-Gauss gradient scheme with a linear interpolation. The divergence integrals are calculated using the Gauss divergence theorem with a linear interpolation scheme. Similarly the Laplacian integrals are computed using the Gauss divergence theorem with a linear interpolation scheme and a corrected surface normal gradient scheme.

Since we are seeking a steady RANS solution of a high-Reynolds number turbulent flow, the 'rhoSimpleFoam' solver of OpenFOAM was used for the simulation. We chose the realizable $K - \epsilon$ turbulence model modified with coefficients from Ref. [23]. The modified realizable $K - \epsilon$ model has been found to yield accurate mean flow prediction [25]. The normalized mean flow velocity obtained from the simulation for the C17M90 case is presented in fig. 3. The coarse and fine grids are giving essentially identical results. Moreover, the mean streamwise velocity profiles are also matching with the reference experimental results [4] up to $x = 10$. As we go further downstream, the RANS solution appears to be more dissipative. Since we are able to obtain the mean flow data accurately within the noise-producing region, the lack of accuracy further downstream might not affect the far-field noise prediction. We can observe similar behaviour in the eccentric jet as well in fig. 4. Here, the accuracy of the mean flow velocity is less compared to the accuracy of the coaxial case.

The centerline Mach number distribution is the sole data available to validate the mean flow of the *heated* coaxial and eccentric jets (for which far-field SPL data are available for validation of our noise prediction tool). The centerline

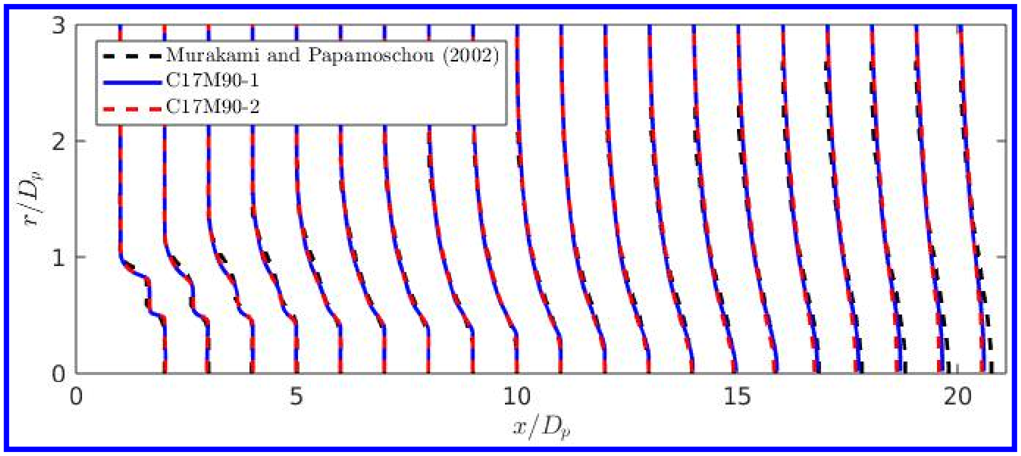

Fig. 3 **Normalized velocity $\overline{u}/U_p$ profiles for C17M90 at various axial locations.**

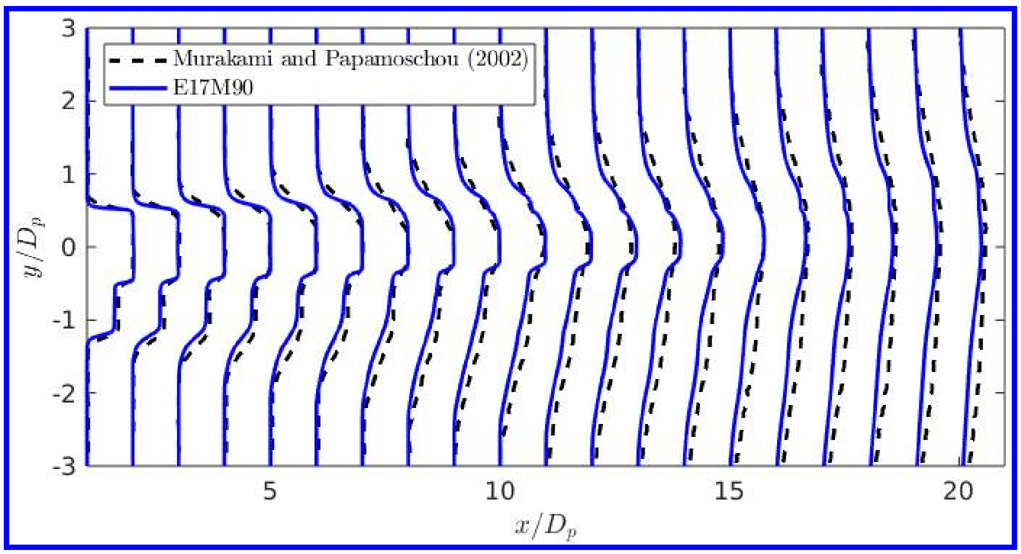

Fig. 4 **Normalized velocity $\overline{u}/U_p$ profiles for E17M90 at various axial locations.**

Mach number distributions along the streamwise direction are presented in fig. 5. The simulation results, labelled as '(RANS)' in the plot, are compared with corresponding experimental data provided in Ref. [3], labelled as '(Exp)'. Despite employing the method of characteristic nozzle to achieve ideally expanded jets, the flow field still exhibits shock cell structures. The single-stream jet simulation result matches the corresponding experimental result closely. However, the dual-stream coaxial and offset jets tend to over-predict the potential core length and exhibit higher dissipation beyond the potential core. The difference in the potential core length between the experiment and the simulation is large for the eccentric case. So, we increased the axial extend of the domain from $20D_p$ to $30D_p$, to see its effect on the mean flow calculation. Comparing the ECC-1 and ECC-2 RANS solution, we could see slight changes in the mean flow prediction after the potential core and slightly less dissipative than the previous grid.

B. Adjoint Green's function

The methodology used for solving Lilley's equation for a non-axisymmetric jet is detailed in II.B. To validate this approach, we compared the non-axisymmetric Green's function calculation with the axisymmetric counterpart for a Mach 1.5 ideally expanded isothermal round jet. We have previously validated the algorithm developed for adjoint Green's function calculation and far-field noise prediction for axisymmetric jets in Refs. [14, 26, 27].

The adjoint Green's function computed using both methods is presented in fig. 6. Here, the sound source is located at $R_0 = 80D_p$, $\Theta_0 = 90^0$, and $\phi_0 = 0^0$ with a Strouhal number of $St = 0.3$. Both the real and imaginary parts of the

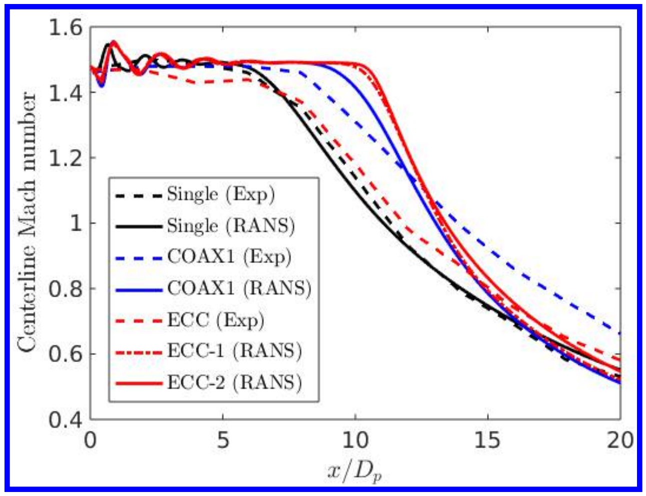

Fig. 5 **Centerline Mach number distributions along the streamwise direction.**

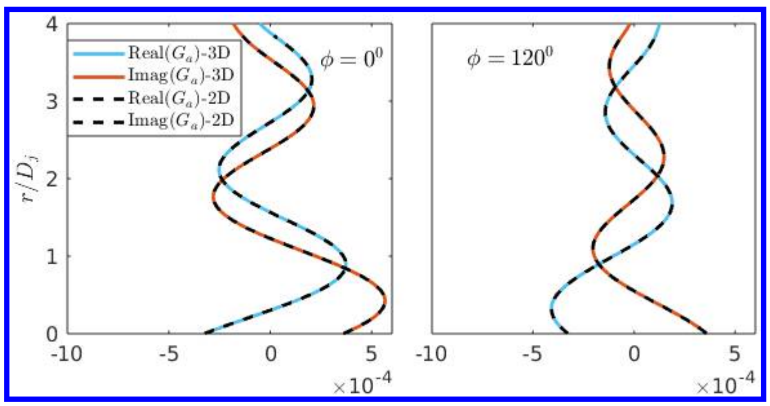

Fig. 6 **Adjoint Green's function computed using the methodology explained in section II.B compared with the axisymmetric calculation [14] for an isothermal ideally expanded Mach 1.5 round jet [28].**

adjoint Green's function are shown within the jet plume location of $x = 2D_p$ and $\phi = 0^0, 120^0$ for all radial locations, including the inner and outer parts of the solution. The non-axisymmetric computation is labeled as '3D', while the axisymmetric computation is labeled as '2D'. It is evident from the figure that the two results match exactly.

We further investigate the effect of eccentricity (e) on the adjoint Green's function. For this analysis, we manufactured a dual-stream jet with Mach 1.5 in the primary and Mach 0.9 in the secondary nozzle. The dual-stream jet mean flow is generated only for a particular axial location by choosing appropriate values of coefficients in a double Gaussian profile [29] for different choices of offset values. The variation of the real part of the adjoint Green's function with offset and source azimuthal location is presented in fig. 7. It is important to note that the source location in the adjoint problem corresponds to the observer location in the direct problem. The results are plotted for a source with a Strouhal number of $St = 0.3$ located at $R_0 = 80D_p$, $\Theta_0 = 90^0$, and $\phi_0 = 0^0, 120^0$.

We observe a smooth transition of the Green's function as we move towards higher eccentricity for both $\phi_0 = 0^0$ and $\phi_0 = 120^0$. Additionally, the magnitudes of the Green's function increase with the rise in eccentricity. The solutions exhibit symmetry about the $\phi = 0^0$ plane for the plane wave coming from the $\phi_0 = 0^0$ case due to symmetry in both the incoming wave towards the jet and the mean flow. However, for the $\phi_0 = 120^0$ case, the adjoint Green's function lacks symmetry with respect to the incoming plane wave, as is to be expected for the non-axisymmetric base flow.

C. Far-field noise

We computed the noise from the Single, COAX1, and ECC-2 jets using the model outlined in Section II. The axial extent of the noise calculation domain is kept consistent with the RANS calculation, reaching up to $25D_p$ for

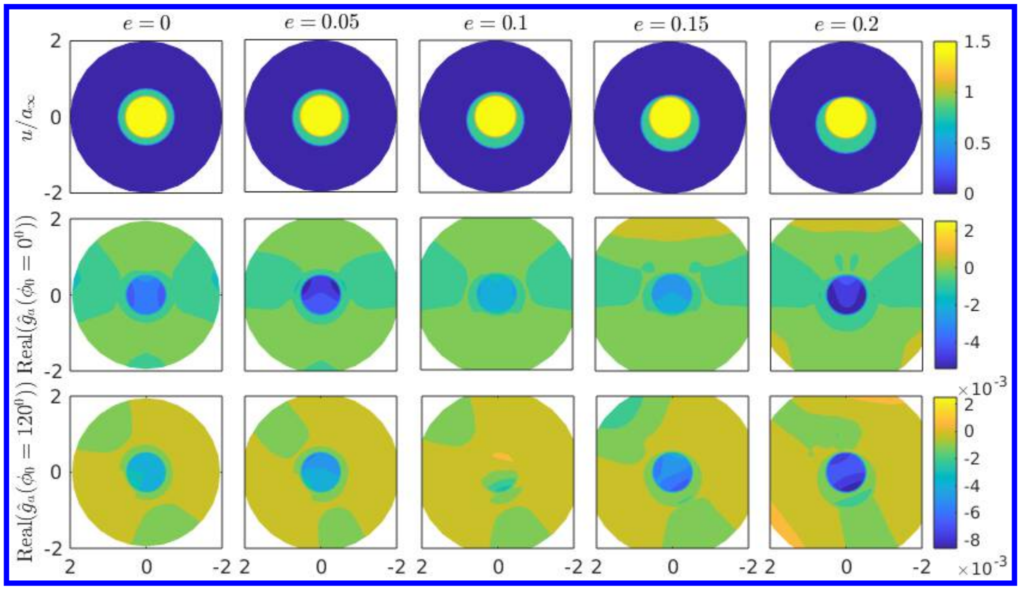

Fig. 7 **Variation of the adjoint Green's function with eccentricity (e) and observer azimuthal location (ϕ_0).**

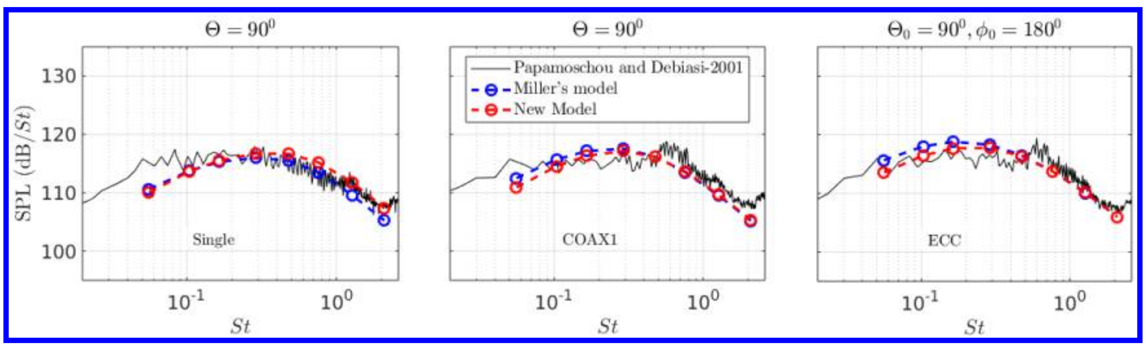

Fig. 8 **Far-field noise predicted using the RANS data for Single, COAX1 and ECC jets for an observer at $R_0 = 80D_p$.**

the axisymmetric jets and $30D_p$ for the eccentric jet. The radial extent of the noise calculation domain varies with the downstream axial location, reaching up to where the inner and outer Green's function solution matches. Length, time, and velocity scales are determined using the mean turbulent kinetic energy and dissipation rate obtained from the RANS simulation, as specified in eqn. (12). We employed two types of frequency-dependent length scale models in the noise prediction. In the first approach we use the frequency-dependent length scale used by Miller [13] (eqn. (13)) and in the second approach we use the model we introduced in our recent study (eqn. (14)).

The far-field noise predicted using these two approaches are presented in fig. 8, where the spectra from the first approach is labelled as 'Miller's model' and the second one is labelled as 'New model'. In the first approach, we selected amplitude coefficients, B_0, and $B_{>0}$, to align with the values presented in Ref. [13]. In the second approach, we re-optimized the values of B_0 and $B_{>0}$ to match the spectra with the experimental data. Re-optimization was necessary because the range of values provided by the existing frequency-dependent length scale model and the new frequency-dependent model differs, as discussed in Ref. [14]. The same set of coefficients is applied to the Single, COAX1, and ECC-2 cases. Although the noise predicted using both models exhibits subtle variations, overall, they align well with the experimental results across a wide range of frequencies. This attests to the essential robustness of the proposed modelling approach that it could be extended in a straightforward manner from axisymmetric jets to non-axisymmetric ones.

We have additional experimental noise data available at $\Theta_0 = 45^0$ only for the eccentric jet. As discussed in Section II.B, the governing equation encounters a singularity at $a_\infty - \overline{u}\cos\Theta_0 = 0$, and $\Theta_0 = 45^0$ falls within this range and we have not predicted the far-field noise at this observer location. Instead, we examine noise predictions from the eccentric

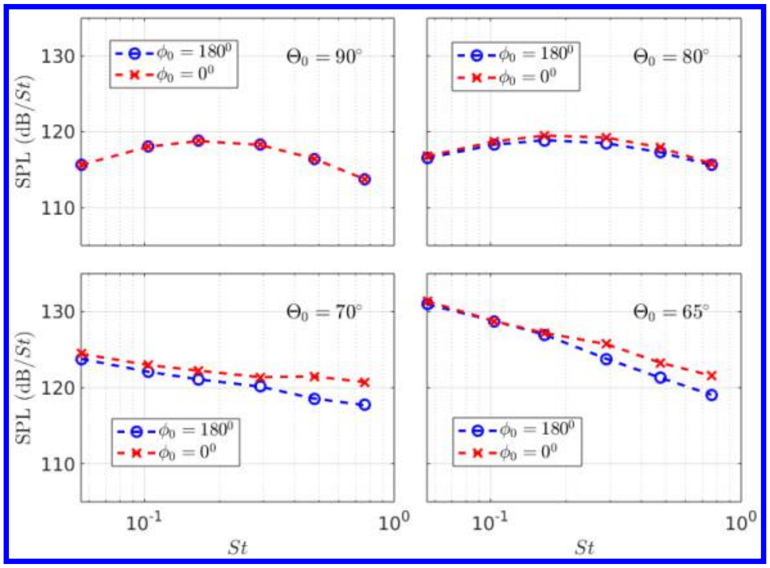

Fig. 9 **Far-field noise predicted using the RANS data for ECC-ϕ_0 jets for an observer at $R_0 = 80D_p$ for various polar observer locations.**

jet at various polar observer locations where the singularity is not encountered (the higher polar angles towards the sideline).

Far-field noise results are presented for observers at $\phi_0 = 180^0$, representing the least noisy region, and $\phi_0 = 0^0$, representing the most noisy region, in fig. 9. From the figure, it is evident that the noise radiated to the 90^0 polar observer location is identical for both $\phi_0 = 0^0$ and $\phi_0 = 180^0$ observer locations. This overlap is expected because the mixing effect of the primary jet with the secondary one does not contribute significantly to higher polar observer locations. Additionally, it can be noted that at $\Theta = 90^0$, the sound pressure level (SPL) data is identical for single-stream, coaxial, and eccentric jets (see fig. 8). As we transition to lower polar observer locations, we observe a suppression of noise radiated towards the $\phi_0 = 180^0$ location compared to the $\phi_0 = 0^0$ location as expected. It is encouraging that our model for the non-axisymmetric jet noise is able to match the expected trend.

IV. Conclusion

Axisymmetric jets serve as the benchmark for most noise studies. However, there is an interest in offset dual-stream round jets for selective noise mitigation in the bottom sector even at the cost of increasing noise radiation to the top sector. Here, we pursue a model based on Lilley's acoustic analogy for the noise radiated by such jets. As in axisymmetric jets, the model requires one to calculate the Green's function of a sound propagation operator and to model the corresponding noise sources. The first part is complicated by the non-axisymmetry of the jets being modeled, but we outline the approach for solving it. On the other hand, the noise sources are modelled based on inputs from a steady RANS simulation, which is also significantly more expensive than for axisymmetric jets.

The basic validation case we conducted for the computation of the non-axisymmetric Green's function involved comparing it to an axisymmetric Green's function calculation where the azimuthal modes are decoupled. Both approaches yielded precisely the same Green's function in the jet plume for an axisymmetric jet. Additionally, we observed a smooth transition of the Green's function with changes in eccentricity and azimuthal observer location. The far-field noise radiated from single-stream, dual-stream coaxial, and offset jets at the sideline angle accurately matched the experimental results reported in the literature. Furthermore, we noted that the noise radiated downwards ($\phi_0 = 180^0$) from the eccentric jet was lower than the noise radiated upwards ($\phi_0 = 0^0$) in the range of downstream polar angles 65° to 80°, but the difference vanishes at the sideline angle. These results serve to partially validate the methodology outlined for predicting the far-field noise of non-axisymmetric jets.

Our future work will focus on augmenting the code to address the critical layer singularity. The lack of this aspect in the current code disallows us from predicting the noise at the physically interesting downstream polar angles. Ultimately, the goal is to provide a rapid- evaluation tool to help in minimization of noise from non-axisymmetric jets of technical relevance.

References

[1] Bridges, J. E., and Brown, C. A., "Parametric testing of chevrons on single flow hot jets," *10th AIAA/CEAS Aeroacoustics Conference, paper 2824*, 2004.

[2] Arakeri, V. H., Krothapalli, A., Siddavaram, V., Alkislar, M. B., and Lourenco, L. M., "On the use of microjets to suppress turbulence in a Mach 0.9 axisymmetric jet," *Journal of Fluid Mechanics*, Vol. 490, 2003, pp. 75–98.

[3] Papamoschou, D., and Debiasi, M., "Directional suppression of noise from a high-speed jet," *AIAA Journal*, Vol. 39, No. 3, 2001, pp. 380–387.

[4] Murakami, E., and Papamoschou, D., "Mean flow development in dual-stream compressible jets," *AIAA Journal*, Vol. 40, No. 6, 2002, pp. 1131–1138.

[5] Papamoschou, D., "New method for jet noise reduction in turbofan engines," *AIAA Journal*, Vol. 42, No. 11, 2004, pp. 2245–2253.

[6] Brown, C., Bridges, J., and Henderson, B., "Offset Stream Technologies Test-Summary of Results," *13th AIAA/CEAS Aeroacoustics Conference (28th AIAA Aeroacoustics Conference)*, 2007.

[7] Henderson, B., Leib, S. J., and Wernet, M. P., "Measurements and predictions of the noise from three-stream Jets," *21st AIAA/CEAS Aeroacoustics Conference, paper 3120*, 2015.

[8] Henderson, B., and Huff, D. L., "The aeroacoustics of offset three-stream jets for future commercial supersonic aircraft," *22nd AIAA/CEAS Aeroacoustics Conference, paper 2992*, 2016.

[9] Tam, C. K. W., and Auriault, L., "Jet mixing noise from fine-scale turbulence," *AIAA Journal*, Vol. 37, No. 2, 1999, pp. 145–153.

[10] Morris, P. J., and Farassat, F., "Acoustic analogy and alternative theories for jet noise prediction," *AIAA Journal*, Vol. 40, No. 4, 2002, pp. 671–680.

[11] Morris, P. J., and Boluriaan, S., "The prediction of jet noise from CFD data," *10th AIAA/CEAS Aeroacoustics Conference, paper 2977*, 2004.

[12] Raizada, N., and Morris, P. J., "Prediction of noise from high speed subsonic jets using an acoustic analogy," *12th AIAA/CEAS Aeroacoustics Conference, paper 2596*, 2006.

[13] Miller, S. A. E., "Toward a comprehensive model of jet noise using an acoustic analogy," *AIAA Journal*, Vol. 52, No. 10, 2014, pp. 2143–2164.

[14] Nadammal Puthiyakath, S., and Sinha, A., "Validation of RANS-Based Jet Noise Prediction Models Using LES," *AIAA SCITECH 2024 Forum*, 2024.

[15] Papamoschou, D., "Modelling of noise reduction in complex multistream jets," *Journal of Fluid Mechanics*, Vol. 834, 2018, pp. 555–599.

[16] Lilley, G. M., "On the noise from jets," Tech. Rep. CP-131, AGARD, 1974.

[17] Tam, C. K. W., and Auriault, L., "Mean flow refraction effects on sound radiated from localized sources in a jet," *Journal of Fluid Mechanics*, Vol. 370, 1998, pp. 149–174.

[18] Abramowitz, M., and Stegun, I. A., *Handbook of mathematical functions with formulas, graphs, and mathematical tables*, Vol. 55, US Government printing office, 1964.

[19] Gudmundsson, K., "Instability wave models of turbulent jets from round and serrated nozzles," Ph.D. thesis, California Institute of Technology, 2010.

[20] Ribner, H. S., "The generation of sound by turbulent jets," *Advances in Applied Mechanics*, Vol. 8, Elsevier, 1964, pp. 103–182.

[21] Morris, P. J., and Zaman, K. B. M. Q., "Velocity measurements in jets with application to noise source modeling," *Journal of Sound and Vibration*, Vol. 329, No. 4, 2010, pp. 394–414.

[22] Pope, S., "An explanation of the turbulent round-jet/plane-jet anomaly," *AIAA journal*, Vol. 16, No. 3, 1978, pp. 279–281.

[23] Thies, A. T., and Tam, C. K., "Computation of turbulent axisymmetric and nonaxisymmetric jet flows using the K-epsilon model," *AIAA journal*, Vol. 34, No. 2, 1996, pp. 309–316.

[24] Geuzaine, C., and Remacle, J.-F., "Gmsh: A 3-D finite element mesh generator with built-in pre-and post-processing facilities," *International journal for numerical methods in engineering*, Vol. 79, No. 11, 2009, pp. 1309–1331.

[25] Kurbatskii, K., "Comparison of RANS Turbulence Models in Numerical Prediction of Chevron Nozzle Jet Flows," *47th AIAA Aerospace Sciences Meeting including The New Horizons Forum and Aerospace Exposition*, 2009.

[26] Nadammal Puthiyakath, S., and Sinha, A., "Comparison of Lighthill's and Lilley's Acoustic Analogies for Jet Noise Modelling," *AIAA AVIATION 2023 Forum*, 2023.

[27] Nadammal Puthiyakath, S., and Sinha, A., "Jet Noise Prediction Using Turbulent Scales from LES and RANS," *Conference on Fluid Mechanics and Fluid Power*, Springer, 2022.

[28] Brès, G. A., Ham, F. E., Nichols, J. W., and Lele, S. K., "Unstructured large-eddy simulations of supersonic jets," *AIAA Journal*, Vol. 55, No. 4, 2017, pp. 1164–1184.

[29] Sohoni, N., and Sinha, A., "Modelling noise sources in offset two-stream jets using linear stability theory," *2018 AIAA/CEAS aeroacoustics conference*, 2018.